metals

MDPI

Article

Production-Related Surface and Subsurface Properties and Fatigue Life of Hybrid Roller Bearing Components

Bernd Breidenstein [1], Berend Denkena [1], Alexander Krödel [1], Vannila Prasanthan [1,*], Gerhard Poll [2], Florian Pape [2] and Timm Coors [2]

[1] Institute of Production Engineering and Machine Tools, Leibniz University Hannover, An der Universität 2, 30823 Garbsen, Germany; breidenstein@ifw.uni-hannover.de (B.B.); denkena@ifw.uni-hannover.de (B.D.); kroedel@ifw.uni-hannover.de (A.K.)

[2] Institute of Machine Design and Tribology, Leibniz University Hannover, An der Universität 1, 30823 Garbsen, Germany; poll@imkt.uni-hannover.de (G.P.); pape@imkt.uni-hannover.de (F.P.); coors@imkt.uni-hannover.de (T.C.)

* Correspondence: prasanthan@ifw.uni-hannover.de; Tel.: +49-511-762-19091

Received: 25 August 2020; Accepted: 3 October 2020; Published: 7 October 2020

Abstract: By combining different materials, for example, high-strength steel and unalloyed structural steel, hybrid components with specifically adapted properties to a certain application can be realized. The mechanical processing, required for production, influences the subsurface properties, which have a deep impact on the lifespan of solid components. However, the influence of machining-induced subsurface properties on the operating behavior of hybrid components with a material transition in axial direction has not been investigated. Therefore, friction-welded hybrid shafts were machined with different process parameters for hard-turning and subsequent deep rolling. After machining, subsurface properties such as residual stresses, microstructures, and hardness of the machined components were analyzed. Significant influencing parameters on surface and subsurface properties identified in analogy experiments are the cutting-edge microgeometry, $\overline{S}$, and the feed, f, during turning. The deep-rolling overlap, u, hardly changes the residual stress depth profile, but it influences the surface roughness strongly. Experimental tests to determine fatigue life under combined rolling and rotating bending stress were carried out. Residual stresses of up to −1000 MPa, at a depth of 200 µm, increased the durability regarding rolling-contact fatigue by 22%, compared to the hard-turned samples. The material transition was not critical for failure.

Keywords: tailored forming; hybrid bearing; residual stresses; X-ray diffraction; rolling contact fatigue; bearing fatigue life

1. Introduction

One of today's challenges in mechanical engineering is the environmentally friendly and resource-saving production of components [1–3]. Moreover, in the fields of energy technology, medical technology, automotive engineering, and the aerospace industry, the requirements for high-performance solid components are increasing steadily [4–6]. In the automotive industry, for example, the aim is to reduce CO_2 emissions by reducing vehicle weight [7,8]. In addition, the development of components with a longer lifetime is one of the most important goals for the industry [9].

The choice of material is, therefore, always based on the requirements of the intended application of the component. Consequently, requirements such as a reduction in weight with a simultaneous increase in mechanical strength cannot be realized with the use of one material. Mono-material

components are thus increasingly reaching their material and production-specific limits. One strategy for reducing the component weight of highly stressed components is to combine different materials in one component. This allows the design of components with different materials that are locally adapted to the respective requirements. In this way, components can be realized that combine partly contradictory properties, such as high mechanical strength and simultaneous weight reduction. This is the focus of the Collaborative Research Centre (CRC) 1153, in which the new process chain, known as "tailored forming", is investigated [10]. In existing production technologies for hybrid solid components, the joining of the components takes place during or after the forming process. In the tailored forming process chain, the components are joined from semi-finished products, at the beginning of the production route, and their properties are specifically influenced by the subsequent forming processes. The simple geometry of the components also facilitates the joining process. In addition, considerably more complex geometries can be produced by this strategy. Within the framework of the CRC, the entire process chain, from the joining of the components until the final machining of the hybrid components, is considered, and the operating behavior of these components is investigated.

In the process chain of solid-part production, machining plays a quality-determining role as the final step. Research results of the last decades show a significant influence of machining on the operating behavior of components due to surface and subsurface modification [11].

In particular, for rolling contacts with high contact stresses >2 GPa, a strong influence on the wear and fatigue life behavior as a function of the surface and subsurface properties is known [12]. In components like roller bearings, an alternating stress field during over-rolling can propagate fatigue-crack growth in the contact zone after high cycle numbers exceeding 10^7 revolutions [13,14]. Component failure occurs when the crack network expands toward the surface, causing spalling of the raceway [15]. Although the topography makes a significant contribution to the operating behavior of components, not all effects can be explained by it. Wear resistance and fatigue life of components are also significantly influenced by residual stresses [11,16]. Residual stresses also have an effect on magnetizability and chemical resistance [17]. In general, compressive residual stresses in the subsurface lead to a proportional increase in fatigue strength [18]. Due to plastic deformations in the subsurface area, the residual stress distributions are of considerable importance, as they have a strong influence on the fatigue limit and the crack initiation tendency of the material. For roller bearings, for example, an increase in fatigue life from 40% to 250% could be achieved by introducing residual compressive stresses [19–23].

However, it must be considered that a residual-stress-induced increase in fatigue strength depends largely on the strength of the material [18]. Denkena et al. were able to show that the probability of failure of roller bearings can be reduced by the targeted introduction of compressive residual stresses [24]. The influences of hard turning and deep rolling was investigated by Pape et al. in terms of bearing fatigue tests. Additionally, an FEM-based model, in combination with a calculation routine, was set up to compute the influence of residual stresses on bearing fatigue [25,26]. However, current research results show that too-high residual compressive stresses can also lead to a shorter service life [27,28]. A cause for this is not yet known and currently represents a research gap [29].

Surface and subsurface properties are significantly influenced by the choice of process parameters and tool microgeometry. The surface roughness is significantly influenced by the feed rate during turning. In addition, cutting speed and tool microgeometry also determine the final roughness of a component [30,31]. The mechanical and thermal effects during chip formation are the main factors influencing the subsurface condition. This can be specifically modified by subsequent processes, such as deep rolling [32]. In interaction with cutting speed and feed rate, the rounding of the cutting edge plays a dominant role in influencing the subsurface. Increasing rounding leads to a higher proportion of material being pressed under the cutting edge. This generally leads to compressive residual stresses below the surface. On the other hand, large cutting-edge radii lead to greater temperature development, which promotes the formation of tensile residual stresses [30,31]. The influence of process parameters

and tool microgeometry on the surface and subsurface properties of hybrid components and their influence on the operating behavior is currently inadequately investigated.

The hybrid design offers the potential to combine contradictory requirements in one component. However, there is no knowledge about the application behavior of hybrid components in comparison to mono-material components. Hence, the aim of this study is to investigate the production-related surface and subsurface properties of tailored forming components in comparison to mono-material components. Research questions that need to be addressed are as follows:

1. Can the surface and subsurface properties be adjusted to a similar extent as for conventional components by varying the cutting parameters?
2. Do the components have the same operating behavior with regard to friction or deflection due to an alternating shear force?
3. Do the same damage mechanisms occur regarding rolling contact fatigue and possible structural failure?
4. Even if the joining zone is not directly loaded in the later application, is it still the weakest point in the component?

For this reason, the joining zone as a weak point of hybrid components is investigated in this work, in comparison to a reference sample set made from monolithic material. A possible influence of the application behavior of hybrid components by modifying the subsurface properties is further examined. A focus is set on the mechanical properties of finished components and their use case as hybrid machine elements under complex loads.

2. Materials and Methods

2.1. Materials

In the presented work, two different steel alloys, SAE5140 and SAE1020, were combined by friction welding. These materials were chosen in order to combine a high-strength steel for highly loaded part zones with a cheaper material for supporting structures. A shaft with material transition in axial direction serves as specimen geometry (see Figure 1a).

For the friction welding process, shafts with a diameter of d = 30 mm, a length of l = 220 mm for SAE1020, and l = 150 mm for SAE5140 were used. As process parameters, a friction speed of n = 2000 min^{-1}, a friction pressure of p = 60 MPa, and a friction path of s = 4 mm were applied. Finally, a compression of p = 150 MPa and a compression time of t = 6 s created the final bond. In the next step, the friction weld bead was removed. Afterward, the friction-welded shafts were impact extruded at a temperature of T = 900 °C, in order to change the bonding zone geometry. Hereafter the hybrid shafts were sawn to a total length of l = 146.5 mm and centered on both sides. The machining process used is divided in two steps. First, the hybrid shafts were roughly turned to an oversized diameter. Then the bearing surface of the pre-turned hybrid shafts was locally hardened at the largest diameter, at a temperature of 860 °C, by an induction hardening process. The heating time was t = 0.5 s, with P = 90 kW. Air and water with a pressure of p = 3 bar each were used for cooling by means of a spray nozzle. The cooling time was t = 15 s. The properties of the materials after the heat treatment are displayed in Figure 1b).

The difference in the hardness of both materials after the heat treatment is evident. SAE5140 is significantly harder than SAE1020 due to the higher carbon content. Therefore, in the finishing operation, different machining behavior of the respective materials is expected. Knowledge about the influence of different material properties on the machining behavior is consequently important in order to comply with shape, dimension, and position tolerances of the hybrid components. In the second and thus final machining step, the hybrid shafts are then turned to size with a required surface quality of Ra = 0.14 µm and with adapted process parameters. With higher roughness values, the load-carrying capacity of the bearings would not be fully utilized, since contacting roughness peaks in the mixed friction area can lead to surface-induced early failures.

a)

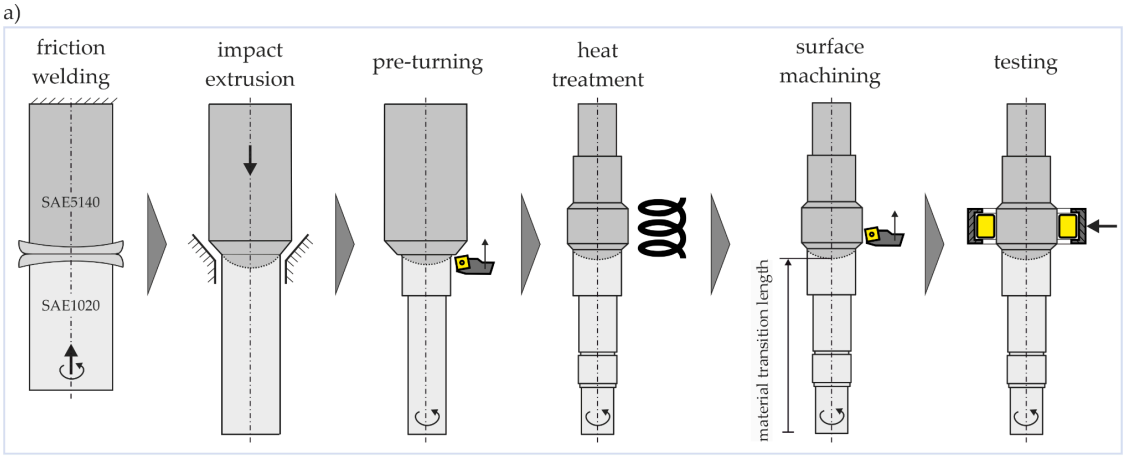

b)

material properties			
		SAE5140	SAE1020
density	g/cm³	7.72	7.87
tensile strength	MPa	1,015.7	1,034.7
yield point	MPa	800	753.7
Young's modulus	GPa	210	200
hardness	HV 1	612	258

material composition						
SAE5140						
Fe 97.2%	Mn 0.7%	C 0.4%	Si 0.2%	Cu 0.2%	Cr 1.0%	other 0.3%
SAE1020						
Fe 98.2%	Mn 0.8%	C 0.2%	Si 0.2%	Cu 0.2%	Cr 0.1%	other 0.3%

Pra/84399 © IFW

Figure 1. (**a**) Process chain for the production of hybrid shafts, and (**b**) material properties and composition.

2.2. Machining

Machining is one of the most important steps in the process chain of manufacturing hybrid components because it determines the final surface and subsurface properties of a component. Therefore, it is essential to understand the influences of the machining parameters on the surface and subsurface properties of hybrid components. In this work, the influence of turning and deep-rolling parameters on these properties were investigated. At first, analogy studies were carried out on simplified component geometries, with friction-welded hybrid shafts of SAE5140 and SAE1020. With the help of analogy studies, correlations and interactions between process parameters and subsurface properties were investigated. Subsequently, with the knowledge of the machining behavior and its influence on the surface and subsurface properties, hybrid shafts with different manufacturing strategies were produced. The operating behavior of these hybrid shafts was then investigated by roller-bearing tests. The results were compared to conventionally manufactured shafts as a reference.

2.2.1. Turning

Analogy experiments with a three-step variation of cutting speed, v_c, and feed, f, were carried out on cylindrical shafts with a material transition in axial direction. Coated indexable cemented tungsten carbide inserts DNMA150612 WAK20 with a symmetric cutting-edge rounding of S_α/S_γ = 30/30 µm, as well as S_α/S_γ = 75/75 µm, were used. Depth of cut, a_p, and cutting direction were kept constant. Process parameters from the analogy investigations that have a significant influence on the subsurface properties were then used for the production of hybrid shafts for fatigue tests. All turning experiments were conducted on a Gildemeister CTX420 linear machine tool (DMG Mori Aktiengesellschaft, Bielefeld, Germany). A rake angle of $\gamma = 3°$ was chosen for the longitudinal turning process. Analogy experiments with different feed directions (machining from hard–soft or soft–hard) on friction welded shafts revealed worse quality for the feed direction from SAE5140 (hard) into SAE1020 (soft) in the machining process. The reason is that clamping of the shaft with the SAE1020 side is inconvenient due to the lower strength of this material. This leads to slight chatter vibrations during

machining. Therefore, in the following investigations, only the feed direction SAE1020 into SAE5140 was selected. The cutting parameters are summarized in Table 1. The choice of cutting parameters for the production of shafts for fatigue-life investigations is based on the lowest achieved roughness.

Table 1. Process parameters of the cutting operation.

Process Parameters	Unit	Analogy Experiments	Final Component
cutting speed, v_c	(m/min)	50–200	180
feed, f	(mm)	0.05–0.2	0.05
depth of cut, a_p	(mm)	0.1	0.1
cutting-edge geometry, S_α/S_γ	(µm)	30/30 and 75/75	30/30 and 75/75
cutting direction,	(-)	SAE1020→SAE5140	SAE1020→SAE5140

2.2.2. Deep Rolling

Additionally, deep rolling experiments were conducted on a CTX420 linear Gildemeister machine tool. For this, the indexable insert of the turning tool was replaced by a hydrostatic rolling tool HG6 with a ball diameter of d_b = 6.35 mm, manufactured by the company ECOROLL AG. Analogy studies were also initially carried out, and the findings were then transferred to the final machining. Before deep rolling, the shafts were turned with the process parameters of the final component, as shown in Table 1, with a cutting-edge geometry of S_α/S_γ = 30 µm. During the deep rolling process, the rolling pressure and the deep rolling speed were kept constant at p_r = 40 MPa and v_w = 180 m/min. The rolling overlap, u, was varied in three steps. Just as for turning, the parameters for fatigue life investigations for deep rolling experiments were also selected according to the best achieved surface quality. The deep rolling direction did not show any significant influence on the surface results. Therefore, the machining direction was chosen analogous to turning. The process parameters for deep rolling are summarized in Table 2.

Table 2. Process parameters of the deep-rolling operation.

Process Parameters	Unit	Analogy Experiments	Final Component
deep rolling speed, v_w	(m/min)	180	180
overlap, u	(%)	50–99	85
deep rolling pressure, p_r	(bar)	400	400
ball diameter, d_b	(mm)	6.35	6.35
deep rolling direction	(-)	SAE1020→SAE5140	SAE1020→SAE5140

2.3. Residual Stress Measurement

Residual stress measurements were carried out via X-ray diffraction (Agfa NDT Pantak Seifert GmbH & Co KG, Ahrensburg, Germany), using the $\sin^2\psi$-method described by Macherauch and Müller [33]. In order to get a non-destructive and depth-resolved measurement of residual stresses, the energy-dispersive measurement method is applied. Here, the determination of lattice strain is also based upon the well-established Bragg's law:

$$n \cdot \lambda = 2 \cdot d_{hkl} \cdot sin\theta_{hkl} \quad (1)$$

where n is a natural number indicating the diffraction order, λ is the X-ray wavelength, d_{hkl} is the interatomic lattice spacing, and θ_{hkl} is the diffraction angle (Bragg angle). For the energy-dispersive measurement, white X-radiation from a tungsten anode tube on a Seifert XRD Space Universal diffractometer is used (Figure 2, left). High depth resolution is achieved at an acceleration voltage of U_a = 50 kV and an anode current of I_a = 60 mA. The Bragg angle, θ, remains constant throughout the measurement, at 20°. Thus, all interference lines are simultaneously determined in one diffraction spectrum (Figure 2, right). The peaks determined by this method represent a function of the wavelength,

λ, or photon energy, E_{ph}. Since the different interference lines are distinguished by different energy levels in the spectrum, they can be referred to different depth information. The more peaks in the direction of increasing photon energy can be evaluated, the more depth information about residual stresses is obtained (Figure 2, right). The collimator used has a diameter of 2 mm. Peak position was analyzed by the center of gravity method. The main difference between the well-established angle dispersive and the energy dispersive methods is that, with the energy-dispersive method, the wavelength or photon energy, λ, is varied at a constant Bragg angle, θ, and in the angle-dispersive method, the Bragg angle, θ, is varied at a constant wavelength, λ. The attainment of residual stress depth information up to 35 µm in the hybrid transition zone of steel is non-destructively possible with a single measurement [34]. In order to get a higher information density in the depth direction, electrolytic removal of material was additionally used. Measurements were done parallel and transverse to the feed direction.

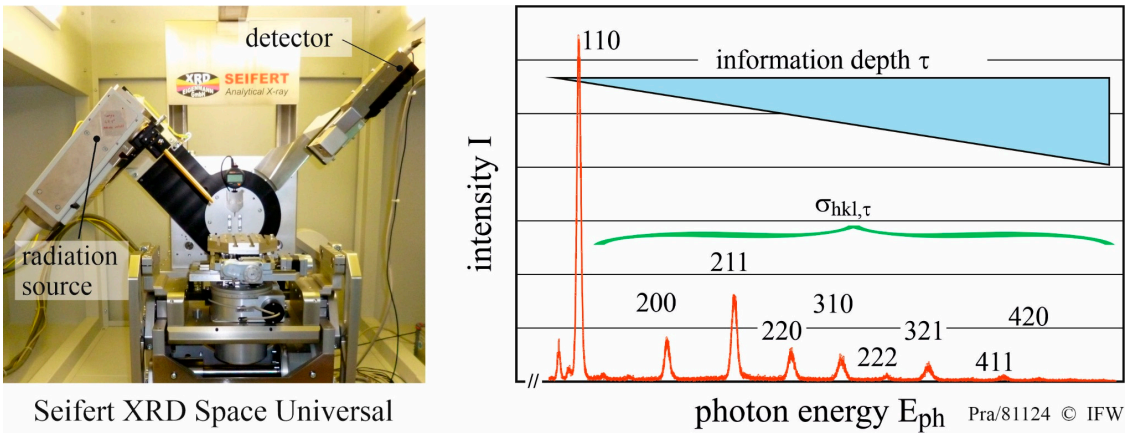

Figure 2. Energy-dispersive residual-stress measurement.

2.4. Fatigue Life Testing

After machining, bearing-fatigue tests were carried out on a test bench, according to Figure 3. The shaft with material transition in axial direction was later used to transmit torque and additional rolling contact stresses of a cylindrical roller bearing with an inner ring integrated into the shaft. Here, the specimen is mounted with two conventional deep groove ball bearings of type 6305 as supporting bearings. The SAE5140-part of the shaft acts as an inner ring for a cylindrical roller bearing (CRB) type RNU204. On the CRB, a radial preload of F = 2 kN is applied through a disc spring assembly. The resulting Hertzian contact stress at the inner race contact is p_{H} = 1.9 GPa. The operating conditions with approximately 2 GPa pressure correspond to medium to high loads for a roller bearing and thus represent the usual operating conditions for shortened life tests. The bearings were lubricated by a temperature-controlled circulating oil lubrication system with a constant volumetric flow rate of $\dot{V}$ = 0.3 L/min per bearing. Additional test parameters are shown in Figure 3, on the right. The radial loading leads to a superposition of rolling-contact stresses and rotating-bending stresses in the contacting surface between the shaft and the rolling element. Within the path of load, measurements using piezoelectric vibration transducers were carried out. In this way, bearing failure during over-rolling of surface spalls was detected by a self-designed condition monitoring system. The tests were automatically stopped if a critical vibration threshold of 150% of the steady state signal was exceeded. A statistical evaluation of the probability of failure of the series was carried out with these lifetimes. After completion of each test, the damage resulting from a surface chipping in the middle of the raceway on the hybrid shaft was documented. The damage and the microstructure were further analyzed by micrographs.

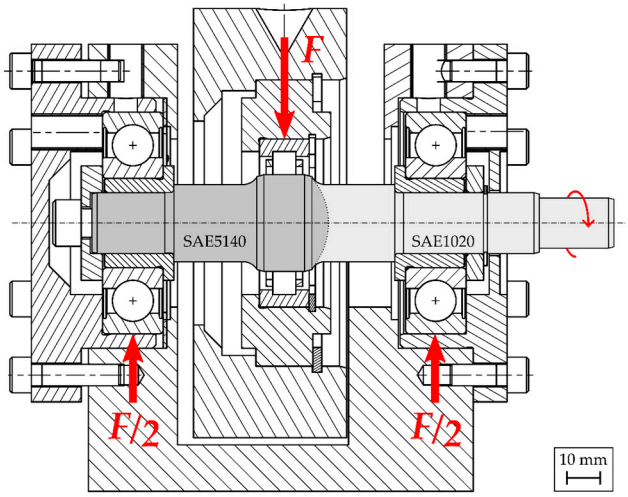

test parameter	unit	value
rotational speed, n_{IR}	(min^{-1})	3,030
radial load, F_{rad}	(N)	2,000
specific load, C/P	(-)	7
contact stress, p_{max}	(GPa)	1.9
viscosity, ν_{40}	(mm2/s)	68
oil temperature, T	(°C)	70
viscosity ratio, κ	(-)	1.8

Figure 3. Fatigue life test in three-bearing arrangement (**left**), and test parameters (**right**).

3. Results and Discussion

In this section, the surface and subsurface properties of the hybrid shafts and the results of the bearing fatigue tests are presented. In turning investigations, only the cutting-edge microgeometry was varied, because it has a decisive influence on the subsurface properties. The cutting-edge microgeometry is defined by the parameters S_γ, S_α, and the form factor κ. At this, S_γ and S_α are the distance between the separation point of the cutting-edge rounding and the tool tip of an ideal sharp cutting at rake face and flank face, respectively. In the presented study, symmetrical cutting-edge roundings, as described in Section 2.2.1, were used. Machining parameters were selected which provide a surface finish with Ra < 0.14 µm as minimum requirement. The knowledge of this was drawn from the analogy studies described above.

3.1. Surface Measurement

Surface roughness plays a decisive role when it comes to the later operating behavior of the hybrid component. Therefore, it is important to identify process parameters that produce a low surface roughness in both materials. Furthermore, it is important to reduce the shape deviation in the transition zone in order to maintain the dimension tolerances of the component.

In Figure 4, the influence of different feeds and microgeometries for turning and overlaps for deep rolling on surface roughness is presented. To investigate the effects of the varied parameters, the surfaces after friction welding and after pre-turning were measured and evaluated. It was ensured that the shafts were pre-turned in the same machining direction and with the same process parameters, in order to achieve a constant initial state before the finishing step of the shafts. The surface analysis after pre-turning showed throughout the investigations an unchanged step in the material transition zone in the range of 12–15 µm, whereby the material range SAE5140 was always higher than SAE1020. The roughness after pre-turning was in the amount of Ra = 0.5–0.6 µm in both material ranges. With decreasing feed, f, it is clearly visible that the roughness decreases, too. The reason for this is that, with the reduction of feed, consecutive roughness peaks are reduced. Consequently, the surface roughness values decrease. However, it can still be observed that the shape deviation in the material transition zone increases with decreasing feed rate. At a feed rate of f = 0.05 mm, the minimum chip thickness is not exceeded in the major part of the chip cross-section, especially in the case of large cutting-edge roundings. As a result, the material is accumulated in front of the cutting edge, and the material is diverted either under the cutting edge into the base material or over the rake face into the chip. This effect, which occurs especially when the chip thickness gets below the minimum chip thickness, is known as the ploughing effect. It is assumed that the properties of the microstructure in the joining zone area of the hybrid shafts are changed by the friction-welding process.

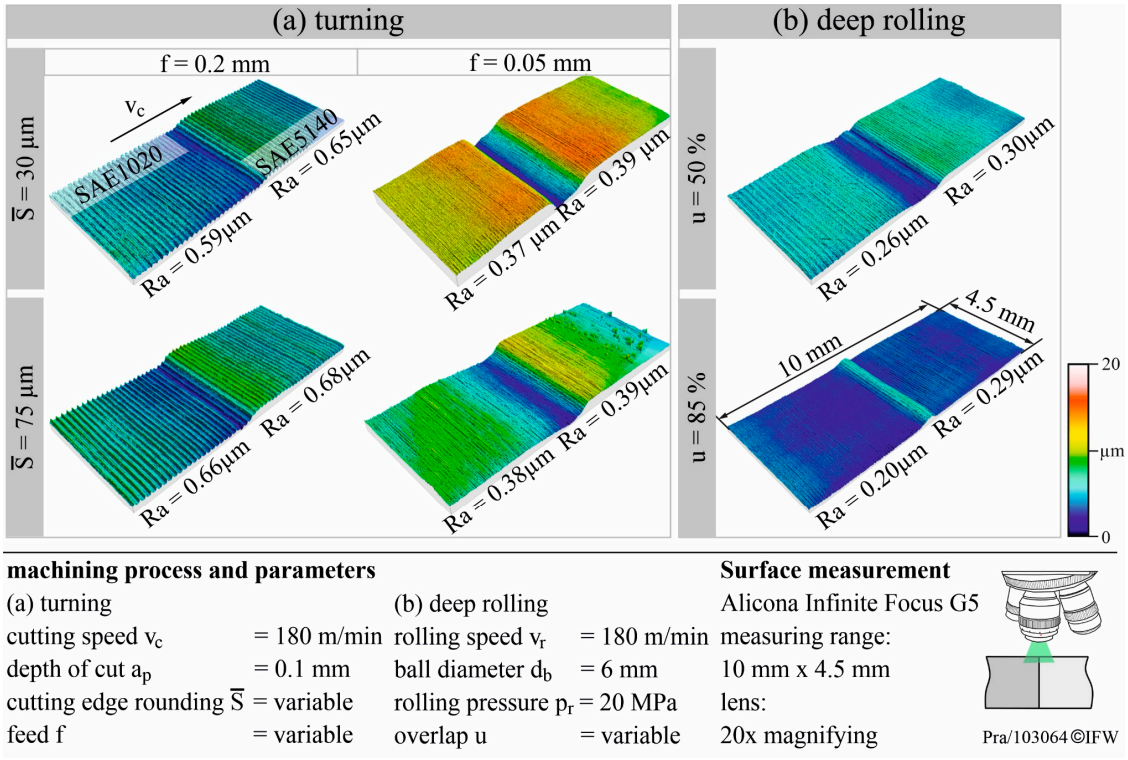

Figure 4. Surface topography and roughness, depending on the machining process (**a**) turning and (**b**) deep rolling.

At low feed rates, this leads to an amplification of the ploughing effect, resulting in a higher indentation depth of the transition zone during turning. In the harder material area of SAE5140, the passive forces increase and leads to a tool displacement. This again increases the workpiece height accordingly. This explains the strongly formed groove for $\overline{S}$ = 30 µm at a feed rate of f = 0.05 mm. With increasing feed, the "weaker" transition area during turning with the higher feed is mainly skipped, so that a step is created, but this is not strongly trough-shaped as with the smaller one. Concerning the influence of the cutting-edge microgeometry on surface roughness, a significant difference between both is not visible. Nearly the same surface roughness values are apparent for both. The shape deviation is smaller by using a cutting-edge rounding of $\overline{S}$ = 75 µm, compared to the cutting-edge rounding of $\overline{S}$ = 30 µm, at a feed of f = 0.05 mm. Here, the mechanical effect exceeds the thermal effect and leads to a smaller shape deviation. The results of the surface roughness measurements for deep rolling show that, with increasing overlap, the surface roughness remains nearly the same, but the shape deviation is significantly reduced. A small shape deviation is only visible in the transition zone. It is apparent that, at an overlap of u = 50%, a groove is formed in the material transition zone, and at an increase of the overlap to u = 85%, in contrast, a small hump is formed. It should be considered that the initial topography before the rolling tests always corresponds to a turned surface with $\overline{S}$ = 30 µm, f = 0.2 mm, and v_c = 180 m/min. According to this, there is always a step in the material transition zone in the initial state before deep rolling. As in turning, deep rolling with an overlap of 50% also causes an indentation of the material due to a changed microstructure and microstructural properties in the material transition zone, as a result of the friction-welding process. If the overlap is increased, however, more material in the soft SAE1020 area is plastically deformed and pushed in front of the ball that the ball nearly fills the step and moreover starts to accumulate into a hump. This is compacted and hardened as the ball passes over it. In the harder SAE5140 area, the material is again densified. As a result, a small hump remains in the material transition zone. However, further, more detailed investigations are necessary to confirm this thesis.

Finally, comparing the surface roughness and topography of the different machining processes of turning and deep rolling, the results are evident. It can be clearly seen that deep rolling produces significantly better surface roughnesses and topographies than turning of hybrid components.

3.2. Microstructure and Hardness

Figure 5 shows the microstructure of the hybrid shafts produced with different machining processes for the fatigue-life investigations. The area influenced by the machining process is significantly larger in the deep rolled specimens than in the turned specimens. The joining zone is not directly located in the bearing raceway but in the area of the chamfer, about 3 mm from the rolling element. The characteristic microstructure of the joining zone due to the extrusion process is also clearly visible. Deep rolling induces higher mechanical stress in a greater material depth, z, which modifies the microstructure to a higher depth. Consequently, in addition to the residual stresses, structural properties are also influenced by different machining processes and must be considered in fatigue tests, too.

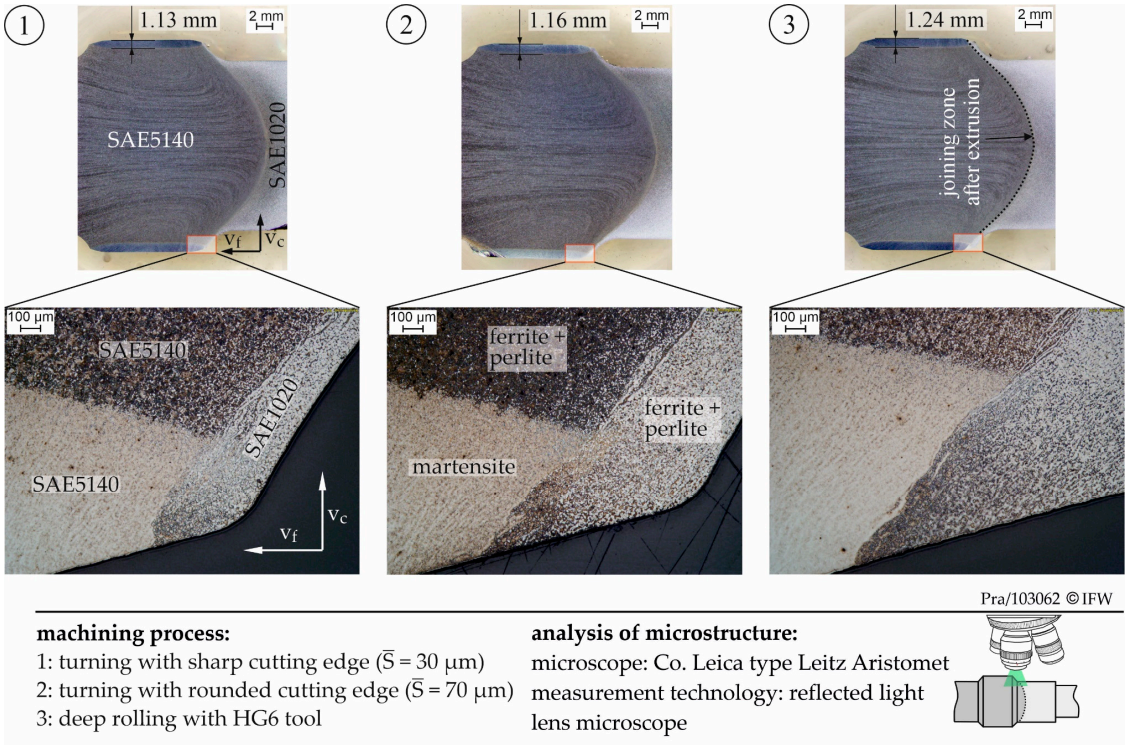

Figure 5. Influence of different manufacturing processes (1) turning with sharp cutting edge, (2) turning with rounded cutting edge and (3) deep rolling on the microstructure of hybrid components.

Hardness measurements were carried out in order to investigate the influence of different processes and their parameters on hardness. In Figure 6, the results are presented. Differences in the hardness values, depending on the machining process, are obvious. The transition to basic hardness depends on the depth of the heat-affected zone during induction heating and lies within the usual process tolerance, cf. Figure 5.

Deep rolling leads to an increase in hardness of the subsurface material. During deep rolling, the material is compacted due to the contact pressure of the rolling tool. This plastic deformation causes an increase in hardness. An influence of different cutting-edge roundings on surface hardness can also be seen. A larger cutting-edge rounding leads to a slight increase in the hardness of the component. This is also due to greater plastic deformation or compaction of the material with larger cutting-edge rounding. Consequently, the investigations show that the machining process influences surface hardness, which can also lead to a different operating behavior of the hybrid component.

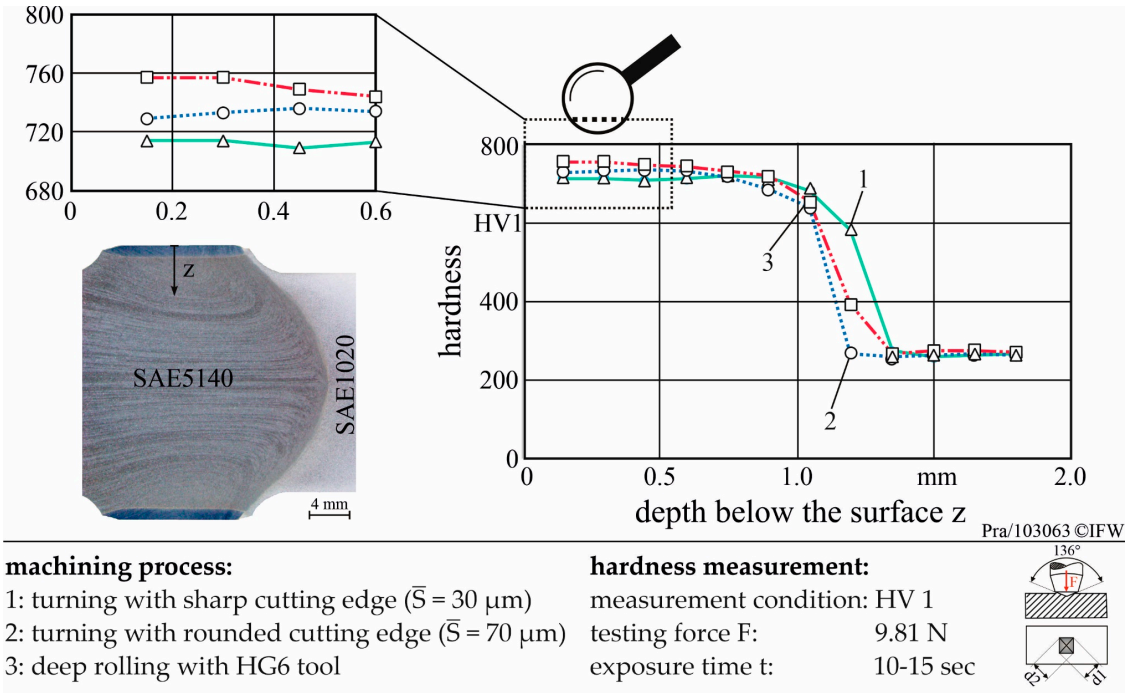

Figure 6. Influence of different manufacturing processes on surface hardness.

3.3. Residual Stresses

In Figure 7, residual stress depth profiles of hybrid components for lifetime investigations, adjusted by turning with different cutting-edge microgeometries and by deep rolling, are displayed. The residual stress measurements were carried out on the bearing running surface, in order to be able to investigate the influence of the subsurface properties on the operating behavior.

The residual stresses were measured both parallel and transverse to the feed direction. For the residual-stress measurements, the energy-dispersive method, in combination with electrolytic-material removal, was used. The procedure is shown schematically on the right side in Figure 7. By first looking at the different machining processes of turning and deep rolling, it is noticeable that, parallel to the feed direction, different courses of the residual stress graphs can be seen. In turned components, on the one hand, maximum compressive residual stresses can be observed near the surface. With increasing depth, z, the residual stress profile has a positive gradient. In deep-rolled components, on the other hand, residual compressive stresses also occur near the surface, but these increase further in the direction of compression with increasing depth. The maximum compressive residual stresses are not surface near. In deep rolling, the maximum elongation is below the surface of the workpiece. Due to the mechanical coupling of the plastically expanded subsurface of the workpiece with the plastically undeformed workpiece environment, compensating strains occur which cause a surface-parallel compression of the plastically deformed subsurface and thus cause residual compressive stresses. Since the maximum strain is below the surface of the workpiece, the maximum plastic deformation also occurs here.

Therefore, the residual compressive stress maximum is also localized in this area. For deep rolling, the mechanical load is much higher than for turning processes. Therefore, higher values for compressive residual stresses are obtained by deep rolling. The residual-stress depth profiles obtained by the variation of cutting-edge roundings ($\overline{S}$ = 30 µm and $\overline{S}$ = 75 µm), show no significant differences. The influence of these different residual-stress depth profiles on the application behavior, especially between turned and deep-rolled samples, was further investigated during fatigue testing.

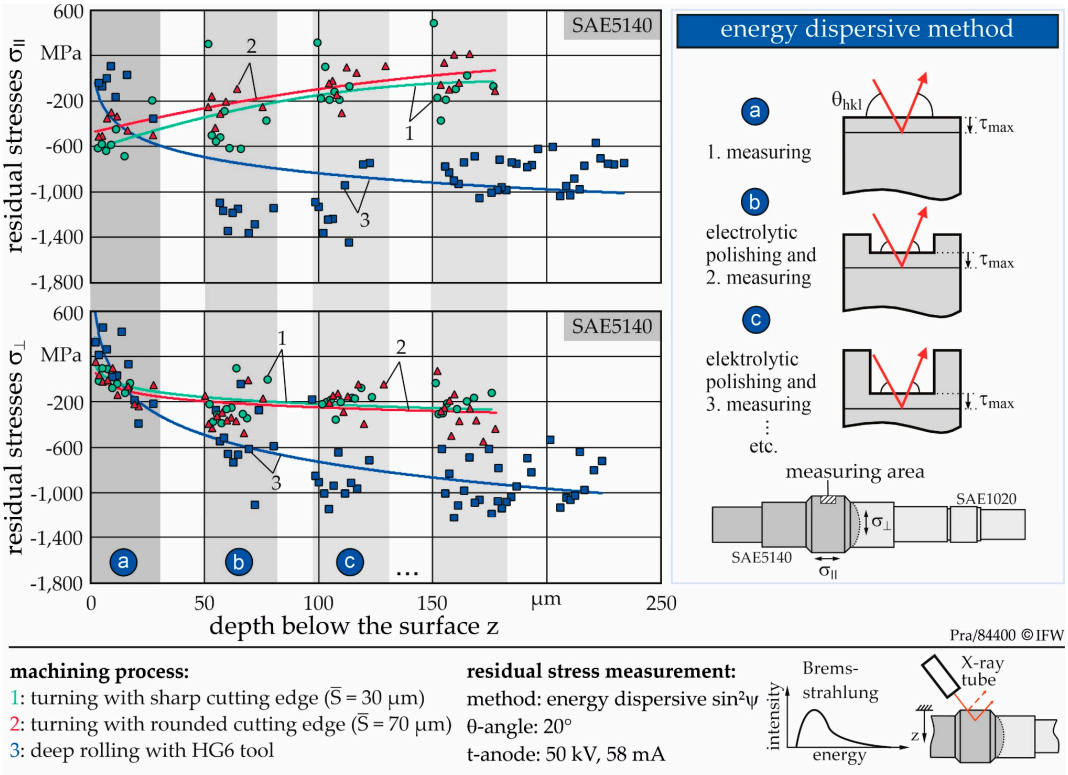

Figure 7. Influence of different manufacturing processes on the residual-stress depth profile measured with the energy dispersive method combined with electrolytic polishing (**a**–**c**).

3.4. Fatigue Life

Figure 8 shows the two-parameter Weibull probability plot [35–38] for bearing fatigue-life testing, using maximum likelihood estimation. Here, the failure probability of four series is plotted against the number of load cycles in terms of inner-ring rotations in a double logarithmic diagram. The three production strategies are illustrated, which had a sample size of $n = 3$ each: turning with sharp and rounded cutting edges, respectively, and deep rolling. The tailored forming shafts were compared to $n = 15$ conventionally produced samples with the same geometry made only from SAE5140 from Reference [36], which were ground after heat treatment. Due to restrictions in test bench operation, a reduced speed of 1250 min^{-1} at 60 °C (κ **=** 1.6) was used for the reference series. The slope of the regression line is named as shape parameter β of the Weibull distribution. This parameter can be understood as a constant that depends on the damage mechanism or fatigue behavior of a system. The characteristic lifetime, L_{63}, also called location parameter, $\hat{T}$, of a series is the time period after which approximately 63.2% of the samples have failed.

For the aforementioned load parameters, a bearing life of $L_{63} = 12 \times 10^6$ revolutions could be determined for the reference series made from monolithic SAE5140. The shape parameter of this Weibull distribution is $\beta = 1.39$, which indicates that the failure rate slightly increases with time, suggesting rolling contact fatigue as the damage mechanism. As expected, the density function shows negative skew. For the roller bearing life of SAE52100 bearing steel under good lubrication conditions ($\kappa \geq 2$), the size of the Weibull exponent ranges from $\beta = 1$ to 1.5 [28,37]. According to Reference [17], a general shape parameter of $\beta = 1.35$ for roller bearings is known, which shows that the conventional reference tests correspond well to the expected values, leading to rolling-contact fatigue.

The hybrid samples manufactured with a sharp cutting edge achieved a bearing life of $L_{63} = 10.4 \times 10^6$ revolutions. This is within an 86% margin of the reference series. A shape parameter of $\beta = 1$ suggests a constant failure rate, which usually indicates random failures. Gleß [39] also carried

out fatigue tests for bearing surfaces with different mechanical surface treatments. For rough surfaces, he achieved significantly lower lifetimes than for surfaces with subsequent finishing.

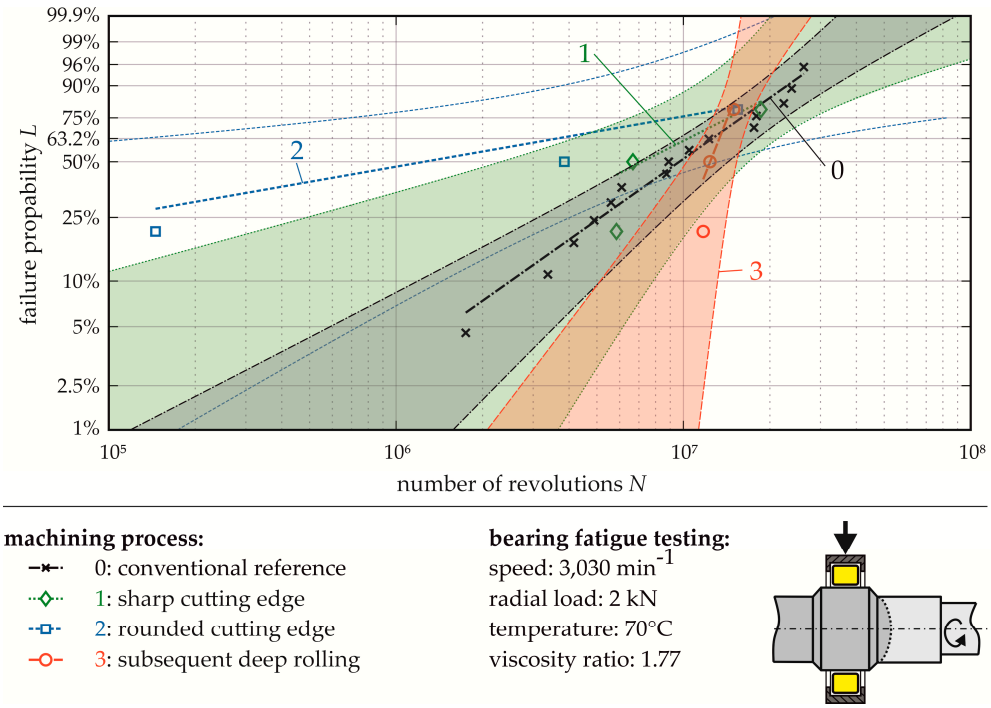

Figure 8. Weibull plots of fatigue-test failures for different machining processes.

During the test series with a rounded cutting edge, an early failure after only 0.15×10^6 revolutions occurred. This results in a bearing fatigue life of $L_{63} = 3.62 \times 10^6$ revolutions, which is only 30% of the reference lifetime. The Weibull slope of $\beta = 0.35$ also indicates early failures with a different mechanism for this series. Due to the small sample number of $n = 3$, this early failure has a strong impact, leading to a very wide confidence interval. The sample set manufactured with rounded cutting edge can therefore not be used for further considerations. Due to comparable lubrication conditions (comparable roughness values), as well as the similar residual stress states in relation to the sample set manufactured with sharp cutting edge, a very similar service life was expected for both test series.

The Weibull plot of the deep-rolled samples shows a relatively steep slope of $\beta = 5$. The samples fail within a short period, resulting in a relatively narrow confidence interval. The confidence intervals of reference dataset and the deep-rolled samples overlap for an interval width in abscissa direction of 4.21×10^6 revolutions at L_{63}. A bearing fatigue life of $L_{63} = 13.34 \times 10^6$ revolutions was achieved. This is 28.5% above the sample set manufactured with sharp cutting-edge geometry and 10% above the reference. Reasons for a lifetime-increasing effect of the rolling process are believed to be improved surface properties, such as higher hardness and especially lower roughness. Microcontacts, which lead to local stress maxima and thus influence surface degradation, can then result in early failures. Various studies have also shown that compressive residual stresses induced by the manufacturing process can extend the fatigue life of roller bearings by a factor of 2.5 [30]. Table 3 summarizes the results of bearing-fatigue testing.

Table 3. Weibull distribution parameters and relative fatigue life to reference samples.

Weibull Parameter	Unit	0: Monolithic Reference	1: Sharp Edge	2: Round Edge	3: Deep Rolling
characteristic life, L_{63}	(10^6 revs.)	12.09	10.38	3.62	13.34
shape parameter, β	(-)	1.39	1	0.35	4.99
relative fatigue life, $\hat{T}_{rel}$	(-)	100%	86%	30%	110%

3.5. Damage Analysis

For each tailored forming production strategy, the sample lying in the middle of the Weibull distribution was examined for damage analysis. Figure 9a shows each spalling damage on the surface which led to the stop of the test with use of laser scanning microscopy. Rolling direction is from bottom to top. The spalls have a size of around 1000 × 500 µm^2 and a maximum depth of −90 to −140 µm. Subsequently, the samples were cut in the longitudinal direction for damage analysis. Figure 9b depicts micrographs of the joining zone and the microstructure in the rolling contact area after fatigue testing. For this, the samples were etched with 2% alcoholic nitric acid.

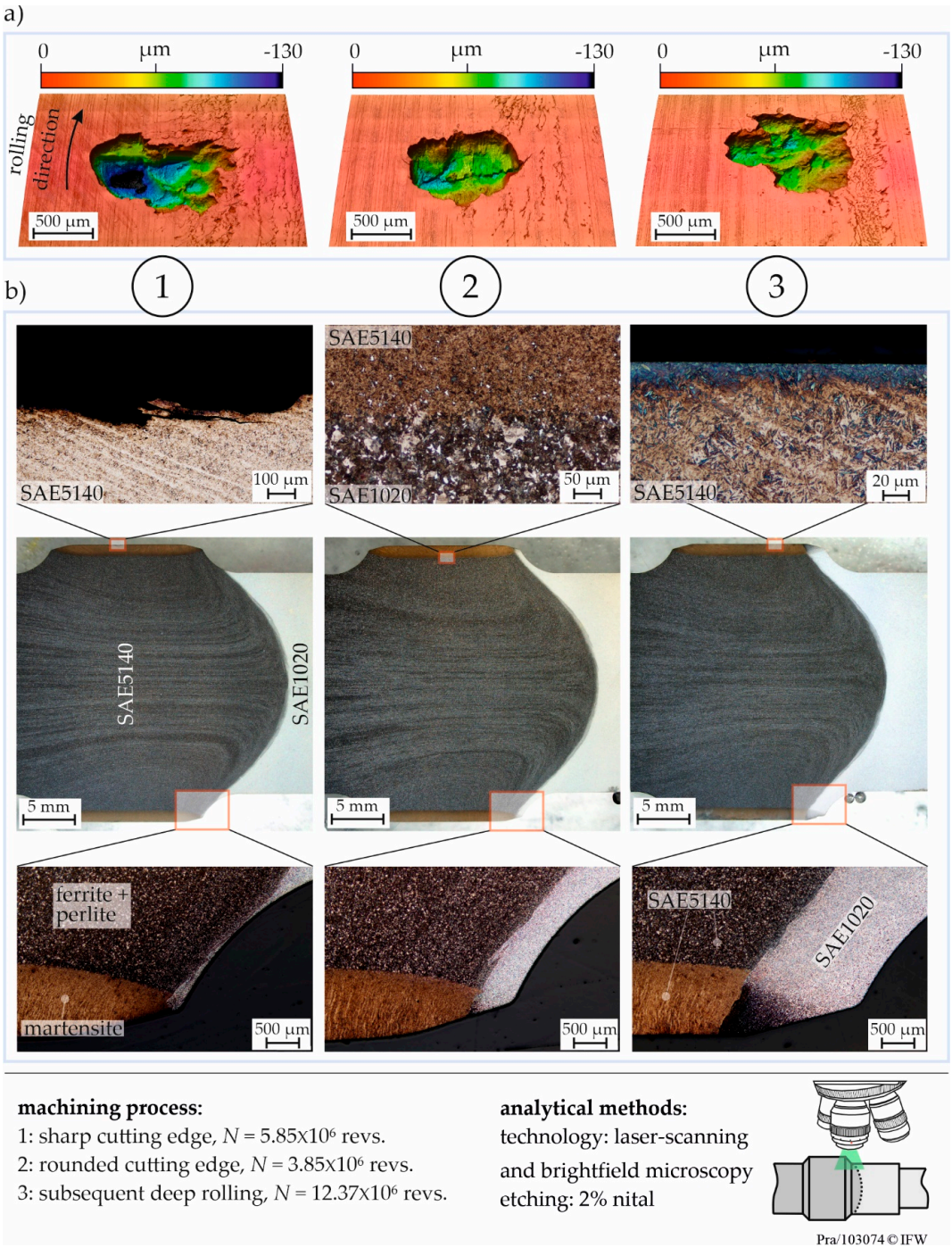

Figure 9. Damage analysis: (**a**) surface laser scanning microscopy of each event-relevant spalling damage, and (**b**) microstructural details in axial section plane.

The depth of the damage lies within the area of maximum orthogonal shear stress induced by the roller bearing. Together with the subsurface crack propagation parallel to the raceway in Figure 9b, this indicates rolling-contact fatigue as the damage mechanism. However, micropittings are visible to the right side of each spall in Figure 9a. Due to the different material properties of the hybrid component, a slightly unevenly shaped deflection of the shaft could cause skewing in the bearing, which, in turn, would result in edge loading. The conventional rolling element features a higher hardness of > 850 HV0.5, which can lead to surface disruption on the shaft. The martensitic microstructure in the hardened area and the ferritic–pearlitic microstructure in the base material are clearly visible in Figure 9b. In the transition zone of these two microstructure areas, some sporadic ferrite grains are visible in the martensitic area. This could be a possible reason for the slightly lower hardness of the martensitic structure. However, structural failure within the joining zone or in the transition zone from the surface-hardened area to the base material did not occur in any of the samples. The test bench-induced alternating bending stress in the joining zone is therefore not critical for the operating parameters presented here.

4. Conclusions and Outlook

The machining and operating behavior of friction welded and extruded hybrid shafts of SAE1020-SAE5140 were investigated. Turning and deep rolling experiments were carried out for manufacturing of the shafts. Subsequently, the influence of different process control variables on the subsurface properties (residual stresses, microstructure, and hardness) was analyzed. For bearing raceways, surface quality is very important in order to exclude failure of the component due to surface defects. Due to this demand, the influence of process parameters on surface roughness and topography were examined first. The feed for turning and overlap for deep rolling have a significant influence on surface roughness. In particular, certain effects occur in the material transition zone, depending on these variables. Depending on the feed rate during turning and overlap during deep rolling, a step, groove, or hump can be observed in the transition area. These are mainly caused by changes in the material properties in the transition area and enhanced by effects such as tool deflection and plastic material deformation. To exclude component failure caused by insufficient surface quality, for further investigations, process parameters which produce the lowest possible surface roughness were selected. In turning experiments, a feed of 0.05 mm, and in deep-rolling experiments an overlap of 85%, were chosen.

The cutting-edge rounding of the tool has a significant influence on the subsurface properties. With increasing cutting-edge rounding, compressive residual stresses are induced. However, deep rolling significantly increases compressive residual stresses regarding induction depth and in terms of residual stress values. In order to investigate the influence of residual stresses on the operating behavior, three different process parameters were used. The hybrid shafts were produced by variation of the cutting-edge rounding in case of turning and by deep rolling. Different cutting-edge roundings led to different sizes of the influenced microstructure area and hardness values in the subsurface. The reason for this is that, with increasing cutting-edge rounding, more material is deformed under the cutting-edge rounding. Deep rolling leads to a further increase of the influenced microstructure area and of surface hardness. The stronger compression of the material results in work hardening and increased hardness. In deep rolling, the observed effects increase even further, since there is hardly any thermal load in this process and the component is thus almost exclusively subjected to mechanical load.

In this first preliminary study to evaluate finishing strategies for tailored forming components, three samples per production strategy were manufactured. Due to the complex production process, a larger sample number, of more than three samples per finishing strategy, was currently not achievable. With the produced samples, fatigue tests were carried out on a bearing fatigue test bench. The aim of the tests was to investigate the fatigue behavior of the hybrid shaft compared to mono-material shafts and, in particular, to highlight the influence of manufacturing processes on the fatigue life

regarding rolling-contact fatigue. Based on the sample series manufactured with sharp cutting-edge geometry, it could be shown that tailored forming machine elements can have a comparable fatigue life to conventional components. An early failure of a sample manufactured with a rounded cutting edge did not allow an evaluation of this series. It seems that an increase in service life can be achieved by additional deep rolling. The reason for this can be improved surface and subsurface properties, such as roughness and hardness. Furthermore, the compressive residual stresses induced seem to have a positive effect on the material microstructure with regard to its fatigue strength behavior. However, it is absolutely necessary to repeat the examinations to confirm this thesis.

In order to further refine the results and, in particular, to increase the empirical significance, the fatigue tests will be continued in the further course of the project. This includes further tests with the same load parameters, as well as other load levels. Thus, different mechanisms of fatigue damage can be provoked, and the manufacturing strategy can be adapted to the later load case. In addition, the production parameters are to be transferred to other tailored forming components with different geometries. This will ensure optimum operating and performance characteristics for future applications of these new high-performance components.

Author Contributions: Designed the machining process, performed the turning and deep rolling experiments, and carried out the analysis of surface and subsurface properties, V.P.; supervised the work, B.D., B.B. and A.K.; designed the samples and carried out the fatigue tests and accompanying analyses, T.C.; supervised the work, G.P. and F.P. All authors have read and agreed to the published version of the manuscript.

Funding: This research was funded by the Deutsche Forschungsgemeinschaft (DFG, German Research Foundation)—CRC 1153—grant number 252662854, in the subprojects B4 and C3.

Acknowledgments: The results presented in this paper were obtained within the Collaborative Research Centre 1153 "Process chain to produce hybrid high-performance components by tailored forming" in subproject B4 and C3. The authors would like to thank the German Research Foundation (DFG) for the financial support of this project. The authors would also like to thank the subprojects B2, B3, A2, and A4 for their support in producing samples through the use of friction welding, impact extrusion, and hardening, as well as in metallographic analysis.

Conflicts of Interest: The authors declare no conflict of interest.

References

1. Giampieri, A.; Ling-Chin, J.; Ma, Z.; Smallbone, A.; Roskilly, A. A review of the current automotive manufacturing practice from an energy perspective. *Appl. Energy* **2020**, *261*, 114074. [CrossRef]
2. Huang, J.; Chang, Q.; Arinez, J.; Xiao, G. A Maintenance and Energy Saving Joint Control Scheme for Sustainable Manufacturing Systems. *Procedia CIRP* **2019**, *80*, 263–268. [CrossRef]
3. Schmidt, M.; Bauer, J.; Haubach, C. Ressourceneffiziente Herstellung mechanischer Verbindungselemente. In *100 Betriebe für Ressourceneffizienz-Band 1*; Springer Spektrum: Berlin/Heidelberg, Germany, 2017; pp. 138–141. [CrossRef]
4. Immarigeon, J.-P.; Holt, R.; Koul, A.; Zhao, L.; Wallace, W.; Beddoes, J. Lightweight materials for aircraft applications. *Mater. Charact.* **1995**, *35*, 41–67. [CrossRef]
5. Sköck-Hartmann, B.; Gries, T. Automotive applications of non-crimp fabric composites. *Non-Crimp Fabr. Compos.* **2011**, 461–480. [CrossRef]
6. Jurczak, P.; Witkowska, J.; Rodziewicz-Motowidlo, S.; Lach, S. Proteins, peptides and peptidomimetics as active agents in implant surface functionalization. *Adv. Colloid Interface Sci.* **2020**, *276*, 102083. [CrossRef]
7. Cole, G.; Sherman, A. Light weight materials for automotive applications. *Mater. Charact.* **1995**, *35*, 3–9. [CrossRef]
8. Padmanabhan, R.; Oliveira, M.C.; Menezes, L.F. *Tailor Welded Blanks for Advanced Manufacturing*; Woodhead Publishing Series in Welding and Other Joining Technologies; Woodhead Publishing Limited: Cambridge, UK, 2011; pp. 97–117. [CrossRef]
9. Fiebig, S.; Sellschopp, J.; Manz, H.; Vietor, T.; Axmann, K.; Schumacher, A. Future challenges for topology optimization for the usage in automotive lightweight design technologies. In Proceedings of the 11th World Congress on Structural and Multidisciplinary Optimization, Sydney, Australia, 7–12 June 2015.

10. Behrens, B.-A.; Bouguecha, A.; Frischkorn, C.; Huskic, A.; Stakhieva, A.; Duran, D. Tailored forming technology for three dimensional components: Approaches to heating and forming. In Proceedings of the 5th Conference on Thermomechanical Processing, Milan, Italy, 26–28 October 2016.
11. Jawahir, I.S.; Brinksmeier, E.; M'Saoubi, R.; Aspinwall, D.; Outeiro, J.; Meyer, D.; Umbrello, D.; Jayal, A.D. Surface integrity in material removal processes: Recent advances. *CIRP Ann.* **2011**, *60*, 603–626. [CrossRef]
12. Nélias, D.; Dumont, M.L.; Champiot, F.; Vincent, A.; Girodin, D.; Fougéres, R.; Flamand, L. Role of Inclusions, Surface Roughness and Operating Conditions on Rolling Contact Fatigue. *J. Tribol.* **1999**, *121*, 240–251. [CrossRef]
13. Olver, A.V. The Mechanism of Rolling Contact Fatigue: An Update. *Proc. Inst. Mech. Eng. Part J J. Eng. Tribol.* **2005**, *219*, 313–330. [CrossRef]
14. Sadeghi, F.; Jalalahmadi, B.; Slack, T.; Raje, N.; Arakere, N.K. A Review of Rolling Contact Fatigue. *J. Tribol.* **2009**, *131*, 041403. [CrossRef]
15. Harris, T.; Kotzalas, M. *Rolling Bearing Analysis*, 5th ed.; CRC Press: Boca Raton, FL, USA, 2006. [CrossRef]
16. Novovic, D.; Dewes, R.; Aspinwall, D.; Voice, W.; Bowen, P. The effect of machined topography and integrity on fatigue life. *Int. J. Mach. Tools Manuf.* **2004**, *44*, 125–134. [CrossRef]
17. Brinksmeier, E.; Cammett, J.; König, W.; Leskovar, P.; Peters, J.; Tönshoff, H. Residual Stresses—Measurement and Causes in Machining Processes. *CIRP Ann.* **1982**, *31*, 491–510. [CrossRef]
18. Sollich, A. *Verbesserung des Dauerschwingverhaltens hochfester Stähle durch gezielte Eigenspannungserzeugung, Fortschrittsberichte VDI*; VDI Verlag: Düsseldorf, Germany, 1994; Volume 5, p. 376.
19. Creţu, S.; Popinceanu, N. The influence of residual stresses induced by plastic deformation on rolling contact fatigue. *Wear* **1985**, *105*, 153–170. [CrossRef]
20. Matsumoto, Y.; Hashimoto, F.; Lahoti, G. Surface Integrity Generated by Precision Hard Turning. *CIRP Ann.* **1999**, *48*, 59–62. [CrossRef]
21. Schwach, D.; Guo, Y.B. A fundamental study on the impact of surface integrity by hard turning on rolling contact fatigue. *Int. J. Fatigue* **2006**, *28*, 1838–1844. [CrossRef]
22. Guo, Y.B.; Warren, A.; Hashimoto, F. The basic relationships between residual stress, white layer, and fatigue life of hard turned and ground surfaces in rolling contact. *CIRP J. Manuf. Sci. Technol.* **2010**, *2*, 129–134. [CrossRef]
23. Choi, Y. A study on the effects of machining-induced residual stress on rolling contact fatigue. *Int. J. Fatigue* **2009**, *31*, 1517–1523. [CrossRef]
24. Denkena, B.; Poll, G.; Maiß, O.; Neubauer, T. Affecting the Life Time of Roller Bearings by an Optimal Surface Integrity Design after Hard Turning and Deep Rolling. *Adv. Mater. Res.* **2014**, *966*, 425–434. [CrossRef]
25. Neubauer, T. Betriebs-und Lebensdauerverhalten Hartgedrehter und Festgewalzter Zylinderrollenlager. Ph.D. Thesis, Leibniz University Hannover, Hanover, Germany, 2016. (In German)
26. Pape, F.; Neubauer, T.; Maiß, O.; Denkena, B.; Poll, G. Influence of Residual Stresses Introduced by Manufacturing Processes on Bearing Endurance Time. *Tribol. Lett.* **2017**, *65*, 87. [CrossRef]
27. Maiß, O. Lebensdauererhöhung von Wälzlagern durch mechanische Bearbeitung. Ph.D. Thesis, Leibniz University Hannover, Hanover, Germany, 2019. (In German)
28. Pape, F.; Coors, T.; Poll, G. Studies on the Influence of Residual Stresses on the Fatigue Life of Rolling Bearings in Dependence on the Production Processes. *Front. Mech. Eng.* **2020**, *6*. [CrossRef]
29. Breidenstein, B.; Denkena, B.; Meyer, K.; Prasanthan, V. Influence of subsurface properties on the application behavior of hybrid components. *Procedia CIRP* **2020**, *87*, 302–308. [CrossRef]
30. Hsu, T.-K.; Zeren, E. Effects of cutting edge geometry, workpiece hardness, feed rate and cutting speed on surface roughness and forces in finish turning of hardened AISI H13 steel. *Int. J. Adv. Manuf. Technol.* **2004**, *25*, 262–269. [CrossRef]
31. Burhanuddin, Y.; Haron, C.H.C.; Ghani, J.A. The Effect of Tool Edge Geometry on Tool Performance and Surface Integrity in Turning Ti-6Al-4V Alloys. *Adv. Mater. Res.* **2011**, 1211–1221. [CrossRef]
32. Abrão, A.M.; Denkena, B.; Breidenstein, B.; Mörke, T. Surface and subsurface alterations induced by deep rolling of hardened AISI 1060 steel. *Prod. Eng.* **2014**, *8*, 551–558. [CrossRef]
33. Macherauch, E.; Müller, P. Das $\sin^2\psi$–Verfahren der röntgenographischen Spannungsmessung. *Zeitschrift für Angewandte Physik* **1961**, *13*, 305–312.

34. Breidenstein, B.; Denkena, B.; Mörke, T.; Prasanthan, V. Non-Destructive Determination of Residual Stress Depth Profiles of Hybrid Components by Energy Dispersive Residual Stress Measurement. *Key Eng. Mater.* **2017**, *742*, 613–620. [CrossRef]
35. Weibull, W. A Statistical Distribution Function of Wide Applicability. *J. Appl. Mech.* **1951**, *103*, 293–297.
36. Coors, T.; Pape, F.; Poll, G. Bearing Fatigue Life of a Multi-Material Shaft with an Integrated Raceway. *Bear. World J.* **2019**, *3*, 23–30.
37. Zaretsky, E.V.; Branzai, E.V. Rolling Bearing Service Life Based on Probable Cause for Removal—A Tutorial. *Tribol. Trans.* **2016**, *60*, 300–312. [CrossRef]
38. Denkena, B.; De Leon, L.; Bassett, E.; Rehe, M. Cutting Edge Preparation by Means of Abrasive Brushing. *Key Eng. Mater.* **2010**, *438*, 1–7. [CrossRef]
39. Gleß, M. Wälzkontaktermüdung bei Mischreibung. Ph.D. Thesis, Otto-von-Guericke-Universität Magdeburg, Magdeburg, Germany, 2009. (In German)